Applied Catalysis B: Environmental 305 (2022) 121070

Contents lists available at ScienceDirect

Applied Catalysis B: Environmental

journal homepage: www.elsevier.com/locate/apcatb

Preparation of oxygen reactivity-tuned FeO_x/BN catalyst for selectively oxidative dehydrogenation of ethylbenzene to styrene

Jian Sheng, Wen-Cui Li, Wen-Duo Lu, Bing Yan, Bin Qiu, Xin-Qian Gao, Rui-Ping Zhang, Shu-Zhen Zhou, An-Hui Lu *

State Key Laboratory of Fine Chemicals, Liaoning Key Laboratory for Catalytic Conversion of Carbon Resources, School of Chemical Engineering, Dalian University of Technology, Dalian 116024, PR China

ARTICLE INFO

Keywords:
FeO_x/BN
Oxygen reactivity
High selectivity
Oxidative dehydrogenation of ethylbenzene

ABSTRACT

Oxidative dehydrogenation of ethylbenzene to styrene is considered to be an eco-friendly process, but suffering from overoxidation of the product to carbon oxides due to uncontrollable oxygen reactivity of the catalysts. Here, we report a boron nitride-supported FeO_x (FeO_x/BN) catalyst, over which an industrially acceptable styrene selectivity (94%) and productivity (0.9 g_{ST} g_{cat}^{-1} h^{-1}) at the conversion of 60% can be attained under oxygen-rich conditions. Based on the investigation of kinetics, CH_3OH-TPD, H_2-TPR, and O_2 pulse reaction, BN support is found to mitigate the oxygen reactivity of FeO_x via the strong interaction between the FeO_x clusters and the BO_x species stemmed from the BN support, which suppresses the overoxidation of ethylbenzene and styrene to carbon oxides. The catalytic tests and structural characterizations reveal that the redox FeO_x species initiate the dehydrogenation and then quinone/carbonyl sites on the newly formed coke deposition over FeO_x/BN catalyst leads to the increase of activity during the induction period. With the aid of the FeO_x and BO_x species, the balance between coke deposition and its gasification rates was achieved under oxygen-rich conditions, guaranteeing stable styrene selectivity and productivity.

1. Introduction

Styrene (ST), an important monomer for polymers in the petrochemical industry, is manufactured by the endothermic dehydrogenation (DH) of ethylbenzene (EB) process over potassium-promoted iron oxide catalysts [1–4]. Since the endothermic and thermodynamically constrained reaction nature, high temperature (600−650 ℃) and excess superheated steam (steam: EB = 6−13:1 in molar) are required to maintain the reaction efficiency and retard the deactivation of the catalyst, which are seriously against the environmentally friendly and sustainable development criterion in the modern chemical industry [5–7]. Oxidative dehydrogenation (ODH) of ethylbenzene to styrene, featured with no thermodynamic equilibrium limitation in conversion, low operation temperature, and free of superheated steam input, is regarded as an eco-friendly alternative to the direct dehydrogenation process [8]. However, overoxidation of styrene or ethylbenzene to carbon oxides is prevalent under high conversion, leading to a low selectivity of styrene, especially over reducible metal oxide catalysts, due to their unmanageable oxygen reactivity [9,10]. Carbonaceous materials with active quinone/carbonyl groups seem to have an appropriate activation of ethylbenzene and oxygen molecules and a high styrene selectivity is obtained [11,12]. However, carbonaceous materials generally suffer from a great risk of burning under oxidative conditions since their inflammable nature [13]. Hence, it is desirable to exploit robust catalysts with a manageable oxygen reactivity, i.e., a matched ability between reduction and reoxidation, to achieve high styrene selectivity and productivity.

Dopants, supports or other unique structures are often used to modulate the oxygen reactivity of reducible metal oxides [14–16]. For example, Mo doping in V_2O_5 increases the binding energy of V−O bonds and inhibits the lattice oxygen evolution for overoxidation, contributing to a high propylene selectivity in the chemical looping oxidative dehydrogenation process [9]. The support effect is also demonstrated to affect oxygen reactivity from both experimental evidence and theoretical study in the oxidative dehydrogenation of propane, including the inverse tendency of TOF values over the specific oxide supports (different bridging V−O−Support bonds) versus their reducibility [10], and the positive correlation between the oxygen defect formation

* Corresponding author.
E-mail address: anhuilu@dlut.edu.cn (A.-H. Lu).

https://doi.org/10.1016/j.apcatb.2022.121070
Received 11 November 2021; Received in revised form 21 December 2021; Accepted 4 January 2022
Available online 6 January 2022

enthalpy and the activation energy of propane [17]. The interaction between metals or metal oxides and supports or promoters, such as strong metal-support interaction (SMSI) and strong metal oxide-oxide support interaction (SOOI), could also alter the oxygen reactivity by the geometric effect and electronic effect [18]. The newly discovered strong metal-support interactions between metals and BN support show a remarkable enhancement in activity and stability for dry reforming of methane reaction [19,20]. Moreover, the interaction between metal ions and high-electron-affinity boric oxide (BO_x) species could lower the oxygen reactivity of metal oxide species [21,22]. These results suggest that the BO_x species seem to play an important role in influencing catalytic behaviors. On the other hand, these BO_x species originated from boron-containing compounds [23–29] or precursors [30–34] are highly selective for the oxidative dehydrogenation of light alkanes and conversion of methane. Our previous study revealed that the BO_x species derived from BN support could modify the activity of MoO_x species to suppress the formation of CO_x in the selective oxidation of ethylbenzene [8], enlightening that the attractive potential in developing highly selective catalysts by incorporating metal oxides and BN support.

In this work, a ball-milling BN supported FeO_x catalyst (FeO_x/BN) exhibits high styrene selectivity and productivity under high conversion level in the oxidative dehydrogenation of ethylbenzene. The strong interaction between metal oxides and BN support has been demonstrated in which FeO_x clusters are covered by BO_x species derived from the BN support under air calcination or ODH reaction process. Such species could regulate the oxygen reactivity of FeO_x species to achieve a matched reduction and reoxidation process in the ODH reaction, leading to a high styrene selectivity. The present findings not only provide a promising catalyst in the production of commodity styrene, but also broaden the SMSI concept from metals and metal oxides over BN support.

2. Experimental

2.1. Chemical reagents

Ferric nitrate ($Fe(NO_3)_3{\cdot}9H_2O$, 99%, Sinopharm) and Silicon carbide (β-SiC, Shanghai Yao Tian) were used as purchased. SBA-15 was synthesized according to the literature [35]. Hexagonal boron nitride (*h*-BN, 99.9%, Aladdin) was ball-milled (Pulverisette 7, Fritsch) with ZrO_2 beads (o.d.: 5 mm) at 800 rpm for 15 min and washed intensively with hot water. The obtained powder was named as BN.

2.2. Catalyst preparation

FeO_x/BN: Supported ferric oxide catalysts were prepared by an incipient-wetness impregnation method. Typically, suitable amounts of ferric nitrate were dissolved in deionized water to an aqueous solution. Then, the solution was incipiently impregnated into BN support and maintained at room temperature for 2 h and dried at 50 ℃ overnight. After calcination in the muffle furnace at 600 ℃ in the air for 2 h, the obtained catalysts were named as y%FeO_x/BN (y represented the amount of Fe, calculated by using the wt% of Fe_2O_3, y = 0.1–9).

1%FeO_x/BN-washed sample was prepared by stirring 1%FeO_x/BN in deionized water at 80 ℃ for 1 h. The resulting suspension was filtered and then dried overnight at 50 ℃ (denoted as 1%FeO_x/BN-washed).

1%FeO_x/BN-x h samples were prepared under ODH reaction for **x hour** time on stream. Reaction conditions: 500 ℃, EB = 5.6 kPa, O_2/EB = 2, N_2 as balance, GHSV = 6000 mL g^{-1} h^{-1}.

1%FeO_x/BN-24 h-H sample was prepared under ODH reaction for 24 h time on stream. And then it was washed with hydrochloric acid (6 M) at 30 ℃ for 6 h to remove the iron species. After centrifugal washing with deionized water to neutral and drying at 50 ℃ for 12 h, the obtained sample was denoted as 1%FeO_x/BN-24 h-H.

Control samples (1%FeO_x/SBA-15 and 1%FeO_x/SiC) were prepared by the same procedures of FeO_x/BN. **Bulk Fe_2O_3** and **BN-600** sample were respectively prepared by the calcination of ferric nitrate and BN support at 600 ℃ for 2 h.

2.3. Catalyst characterization

X-ray powder diffraction (XRD) was measured on an X′Pert-3 Powder diffractometer (PANalytical, Cu Kα, λ = 0.15406 nm). Nitrogen adsorption isotherms (ASAP 3000, Micromeritics) were tested at − 196 ℃. The specific surface areas (S_{BET}) were calculated by the BET method. The UV–vis diffuse reflectance spectra (UV–vis DRS) were collected using $BaSO_4$ as a reference with a diffuse reflectance integration sphere attachment (Internal DRA 2500, Agilent Cary 5000 UV–vis-NIR). Transmission electron microscopy (TEM) images were recorded on a Tecnai G2 F30 S-Twin (accelerating voltage of 300 kV). H_2-TPR and NH_3-TPD were tested on a Micromeritics AutoChem II 2920 apparatus with a TCD detector and/or a mass spectrometer. Before H_2-TPR, the samples were pretreated at 150 ℃ for 1 h under Ar flow and then cooled to ambient temperature under Ar flow, then TPR was performed in the 8%H_2/Ar (50 mL min^{-1}, 10 °C min^{-1}) up to 800 °C. In the case of NH_3-TPD, the sample was pretreated in a flow of He (30 mL min^{-1}) at 500 °C for 1 h. After the temperature was cooled to 100 °C, the sample was pulsed by NH_3 gas. After He purging for 1 h, TPD was performed in He flow (30 mL min^{-1}) at a heating rate of 10 °C min^{-1}. The desorbed mixture was monitored by a TCD detector and an on-line mass spectrometer. CH_3OH-TPD was measured at a homemade apparatus in the following steps: The catalysts (100 mg) were pretreated in a flow of 20% O_2/80%He (25 mL min^{-1}) at 400 °C for 1 h. After the temperature cooled to 50 °C in He and then purged for 1 h, the samples adsorbed CH_3OH for 0.5 h. After He purging for 1 h, TPD was performed in He flow (25 mL min^{-1}) at a heating rate of 10 °C min^{-1}. The desorbed mixture was monitored by an on-line mass spectrometer. Thermogravimetric analysis (STA 449 F3 Jupiter, NETZSCH) was measured from 40 to 800 ℃ under an airflow (40 mL min^{-1}, 10 ℃ min^{-1}). X-ray photoelectron spectroscopy (XPS) was measured on a Thermo Scientific K-Alpha spectrometer (Al Kα X-ray source). The binding energy was calibrated using the C 1 s photoelectron peak at 284.8 eV.

2.4. Catalytic tests

Catalytic tests were carried out in a fix-bed quartz tube reactor (i.d. 8 mm, length 420 mm) using 100 mg catalyst under atmospheric pressure in the temperature range of 450–530 ℃. The reactant (5.6 kPa EB, N_2 as balance) at the total flow rate of 10 mL min^{-1} was fed into the reactor through a saturator (54 ℃). The effluent stream compositions were analyzed by an on-line gas chromatograph (GC7900, Themcomp) equipped with TCD and FID detectors. Heyesep D and molecular sieve 5 A column were attached to TCD, analyzing O_2, N_2, CO, and CO_2; while a PEG capillary column was attached to FID, analyzing hydrocarbons and oxygenates (ethylbenzene, styrene, benzene, benzaldehyde, etc.). The catalytic data were calculated by the following equations:

$$X_{EB}(\%) = \frac{\sum n_i^{out}}{n_{EB}^{out} + \sum n_i^{out}} \times 100$$

$$X_{O2}(\%) = \frac{n_{O2}^{in} - n_{O2}^{out}}{n_{O2}^{in}} \times 100$$

$$S_i(\%) = \frac{n_i^{out}}{\sum n_i^{out}} \times 100$$

$$r = \frac{X_{EB} \times n_{EB}^{in}}{m_{cat}}$$

$$r_{ST} = \frac{X_{EB} \times S_{ST} \times n_{EB}^{in}}{m_{cat}}$$

$$Carbon\ \ balance = \frac{\sum moles\ \ of\ \ carbon\ \ in\ \ outlet}{\sum mols\ \ of\ \ carbon\ \ in\ \ feed}$$

where n_i is the partial mole of the products obtained during the oxidative dehydrogenation of ethylbenzene (styrene, benzaldehyde, benzene, CO, and CO_2). The carbon balance was close to100 ± 5% in all runs and the EB conversion of the blank experiment (quartz sand) was lower than 1% in the whole test temperature range. The mass and heat transfer limitations were accordingly evaluated by Weisz-Prater and Mears' criterion (detailed calculation in SI) [36].

3. Results

3.1. Catalytic behavior of FeO_x/BN

Table 1 showed the catalytic performance of the supported FeO_x catalysts for the oxidative dehydrogenation of ethylbenzene. For the 1% FeO_x/BN sample, an initial EB conversion of 20% with a high ST selectivity of 87% was observed. The control samples 1%FeO_x/SBA-15% and 1%FeO_x/SiC exhibited a high initial EB conversion (~42%) but a low ST selectivity of 68% and 80%, respectively. Notably, the O_2 conversion over the 1%FeO_x/BN catalyst was 16%, while a 100% O_2 conversion was observed over 1%FeO_x/SBA-15, 1%FeO_x/SiC catalysts, and bulk Fe_2O_3. Considering the initial selectivity of CO_x and O_2 conversion over these iron oxide-based catalysts, the 1%FeO_x/BN appeared to have a moderate oxygen activation process and suppressed the overoxidation reaction of ethylbenzene or styrene, thus showing a high selectivity of styrene. As shown in Fig. S1A and B, both EB conversion and ST selectivity increased with time on stream over 1%FeO_x/BN and 1%FeO_x/SBA-15 catalysts. After the induction period, a stable EB conversion (60% vs 60%) and ST selectivity (94% vs 85%) were observed. This induction phenomenon could be attributed to the coke deposition with newly formed active sites (quinone/carbonyl groups) [37,38], leading to an increase in conversion. The increased ST selectivity could be ascribed to the partial coverage of sites for overoxidation. Interestingly, the O_2 conversion over 1%FeO_x/BN catalyst gradually increased and then maintained at ~40% level, while a 100% O_2 conversion was maintained across the tested period over the 1%FeO_x/SBA-15, 1%FeO_x/SiC, and bulk Fe_2O_3 (Table 1).

As shown in Table 1, the catalytic performances of the FeO_x/BN catalysts with different loading amounts of iron oxide were further investigated. The BN support and the calcined BN at 600 ℃ in the air (denoted as BN-600) were tested for EB ODH (Fig. S2). There was an induction period of ~10 h prior to achieving a stable EB conversion over BN-600. This induction phenomenon was similar to the oxidative dehydrogenation of light alkanes catalyzed by BN [39–41]. After the induction period, BN-600 delivered ~11% EB conversion and 78% ST selectivity, along with 13% benzaldehyde selectivity. These results suggested that BN-600 could only afford a relatively poor activity. As for FeO_x/BN samples, the initial EB conversion and O_2 conversion exhibited a direct proportion relation to the loading amounts of iron oxide, while the corresponding ST selectivity was in a contrary tendency (Fig. S2), suggesting that the FeO_x species played a more important role in activity than BO_x species. Also, a stable catalytic performance was observed after an induction period over all the FeO_x/BN catalysts and the ST productivity increased in the sequence 0.1%FeO_x/BN (0.22 g_{ST} g_{cat}^{-1} h^{-1}) < 9%FeO_x/BN (0.72 g_{ST} g_{cat}^{-1} h^{-1}) = 3%FeO_x/BN (0.72 g_{ST} g_{cat}^{-1} h^{-1}) < 1%FeO_x/BN (0.87 g_{ST} g_{cat}^{-1} h^{-1}). A comparative summary of catalytic performance for the oxidative dehydrogenation of ethylbenzene was listed in Table S1. Compared with the reported catalysts, the 1% FeO_x/BN catalyst provided a high styrene selectivity (94%) and productivity (0.87 g_{ST} g_{cat}^{-1} h^{-1}) at a high ethylbenzene conversion (60%), which is close to the commercially attractive productivity (1 $g_{product}$ g_{cat}^{-1} h^{-1}) [42], showing the unique effect of boron nitride support in the oxidative dehydrogenation reaction and the potential in the production of commodity styrene. As for another classical oCNT materials for EB ODH, BN support possesses high thermal conductivity (~33 W m^{-1} K^{-1}), which is beneficial for timely transferring the reaction heat from the reactor to heat exchanger, reducing the generation of hot spots [43]. The excellent oxidation resistance of BN also allows the FeO_x/BN catalyst to tolerate the harsh oxidative conditions, such as a higher oxygen concentration. These features of FeO_x/BN catalyst seem to make it more durable than classical oCNT materials for EB ODH.

As shown in Fig. 1A, the durability of 1%FeO_x/BN catalyst was demonstrated under the switched DH and ODH reaction conditions. Only 0.4% EB conversion was observed in the first DH time on stream. Upon introducing oxygen, the EB conversion dramatically increased to 12% owing to the favorable thermodynamics (Fig. S3). After a 10 h′ induction period, a stable catalytic performance (EB conversion: 60%; ST selectivity: 94%) was observed. However, after switching off O_2, the EB conversion sharply decreased from 60% to 6% within 0.5 h. The residual activity was likely derived from the direct dehydrogenation of ethylbenzene over the active quinone/carbonyl sites [5,38,44]. And the rapid deactivation was possibly due to the reduction of active quinone/carbonyl sites by EB, which was consistent with the literature [45]. As oxygen was introduced again, after a short induction period (2–3 h), the EB conversion and ST selectivity reached a stable state and a similar level as the first ODH region. The EB conversion and ST selectivity showed an excellent reproducibility for 75 h under the next switch of DH and ODH reaction conditions, suggesting the remarkable durability of 1%FeO_x/BN catalyst in the production of styrene.

The evolution of 1%FeO_x/BN catalyst during the induction period was further studied. Fig. 1B showed that the amount of net coke deposition increased and then tended to be stable, while the net coke deposition rate decreased and then plateaued with time on stream. The amount of net coke deposition could be regarded as the difference between intrinsic coke deposition and gasification. This suggested that a balance between coke deposition rate and the gasification rate of coke deposition was gradually achieved in the induction period, which was consistent with the literature findings [46]. Fig. S4 showed the time-on-stream carbon balance of typical FeO_x/BN catalysts (1% FeO_x/BN and 9%FeO_x/BN) during EB ODH process. The carbon balance

Table 1
Catalytic performance of oxidative dehydrogenation of ethylbenzene over supported FeO_x catalysts.

Catalysts[a]	X_{EB} (%)		X_{O2} (%)		S_{ST} (%)		S_{COx} (%)		S_{BZ} (%)		S_{BA} (%)	
	ini[b]	fin[c]	ini[b]	fin[c]	ini[b]	fin[c]	ini[b]	fin[c]	ini[b]	fin[c]	ini[b]	fin[c]
1%FeO_x/BN	20	60	16	40	87	94	5	3	0.8	0.4	4	1
1%FeO_x/SBA-15	42	60	100	100	68	85	23	10	3.5	1.5	2.5	0.5
1%FeO_x/SiC	42	40[d]	100	100[d]	80	77[d]	18	21[d]	1	0.5[d]	1	1.5[d]
0.1%FeO_x/BN	6.5	15	~1	~5	92.5	98	2.5	0.7	1	0	1.5	0
3%FeO_x/BN	24	47	26	42	84	92	10	6	0.6	0.4	4	0.6
9%FeO_x/BN	30	50	43	57	84	89	10.5	9.5	0.6	0.6	2.5	0.5
bulk Fe_2O_3	44	33[e]	100	100[e]	68	61.5[e]	30	37[e]	2	1.5[e]	–	–
BN	4	2	1	1	94	100	6	0	0	0	0	0

a: reaction conditions: 100 mg, 500 ℃, EB = 5.6 kPa, O_2/EB = 2, N_2 as balance, GHSV = 6000 mL g^{-1} h^{-1}; b: initial conversion, time on stream for 0.5 h; c: finial conversion, time on stream for 24 h; d: finial conversion, time on stream for 16 h; e: finial conversion, time on stream for 3.5 h.

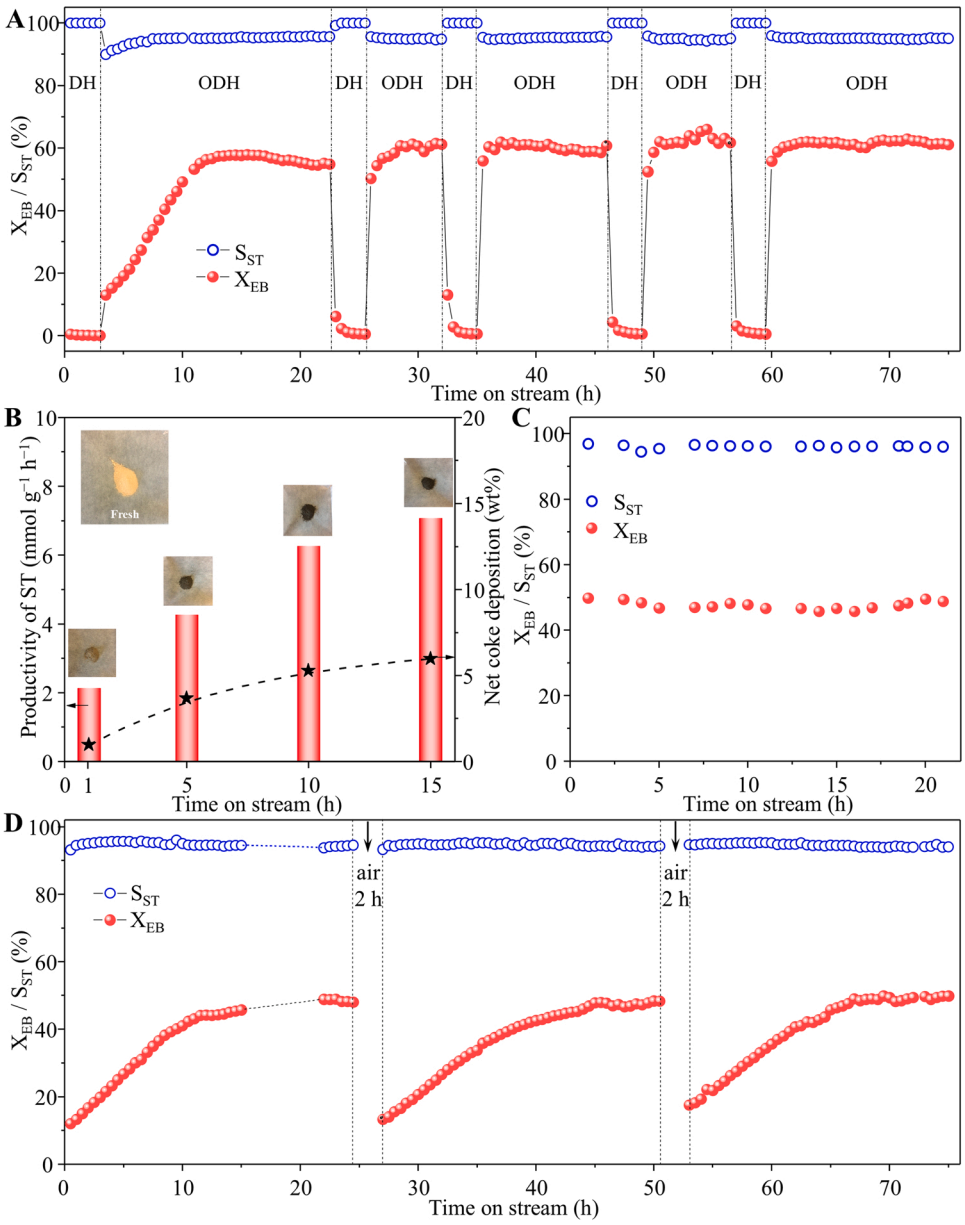

Fig. 1. Time-on-stream catalytic behavior over 1%FeO_x/BN. (A) Catalytic performance under the switched DH and ODH atmosphere. (B) Amount of net coke deposition with time on stream. (C) Catalytic performance over pre-coking 1%FeO_x/BN catalyst. Pre-coking conditions: 500 ℃, ST = 3.2 kPa, O_2/ST = 3, N_2 as balance, GHSV = 6000 mL g^{-1} h^{-1}, 6 h. In situ regeneration conditions: 500 ℃, air of 20 mL min^{-1}, 2 h. Reaction conditions: 500 ℃, EB = 5.6 kPa, O_2/EB = 0 (DH) or O_2/EB = 2 (ODH), N_2 as balance, GHSV = 6000 mL g^{-1} h^{-1}.

could be divided into two stages: At the first stage, mainly during the induction period, the carbon balance was gradually increased from 85% to 95%, indicating that the net rate of coke deposition was gradually mitigated. At the second stage, mainly during the quasi-stationary period, the carbon balance was maintained a relatively stable level (~97%), suggesting that the balance between coke deposition rate and the gasification rate of coke deposition was established, which were well consistent with the results in Fig. 1B. Meanwhile, the productivity of ST also showed a positive correlation with the amount of net coke deposition. Given the possible precursor for coke deposition, styrene was selected to prepare the pre-coking 1%FeO_x/BN catalyst. Over this catalyst (Fig. 1C), a stable EB conversion and ST selectivity without induction period was observed, indicating that the induction period was likely caused by the coke deposition from styrene. An in situ regeneration procedure (500 ℃ under synthetic air for 2 h) in the reactor was also used to evaluate the role of coke deposition (Fig. 1D and S5). The coincident catalytic performance after the twice in situ regeneration procedure suggested that the coke deposition played an important role in enhancing activity and also demonstrated the durability of 1% FeO_x/BN catalyst.

3.2. *Kinetic studies of FeO_x/BN*

As shown in Fig. 2A, the effect of the contact time (W/F) on the conversion of ethylbenzene to various products was further investigated. Over the 1%FeO_x/BN catalyst, the selectivity of styrene increased significantly to near 100% and that to CO_x decreased to zero as the contact time decreased. Styrene could be formed as the exclusive product at the very initial reaction stage over this catalyst, suggesting that styrene was the primary product whereas CO_x was the secondary product. In other words, the reaction channel of direct oxidation of ethylbenzene to CO_x was suppressed by 1%FeO_x/BN catalyst. On the other hand, over the FeO_x/SBA-15 and FeO_x/SiC catalyst, styrene selectivity increased to ~85% and the CO_x selectivity decreased to ~10% with decreasing the contact time to zero. Thus, both styrene and CO_x were the major primary products, indicating the existence of direct oxidation of ethylbenzene to CO_x over both the FeO_x/SBA-15 and FeO_x/SiC catalyst. Besides, the slope between CO_x selectivity and contact time

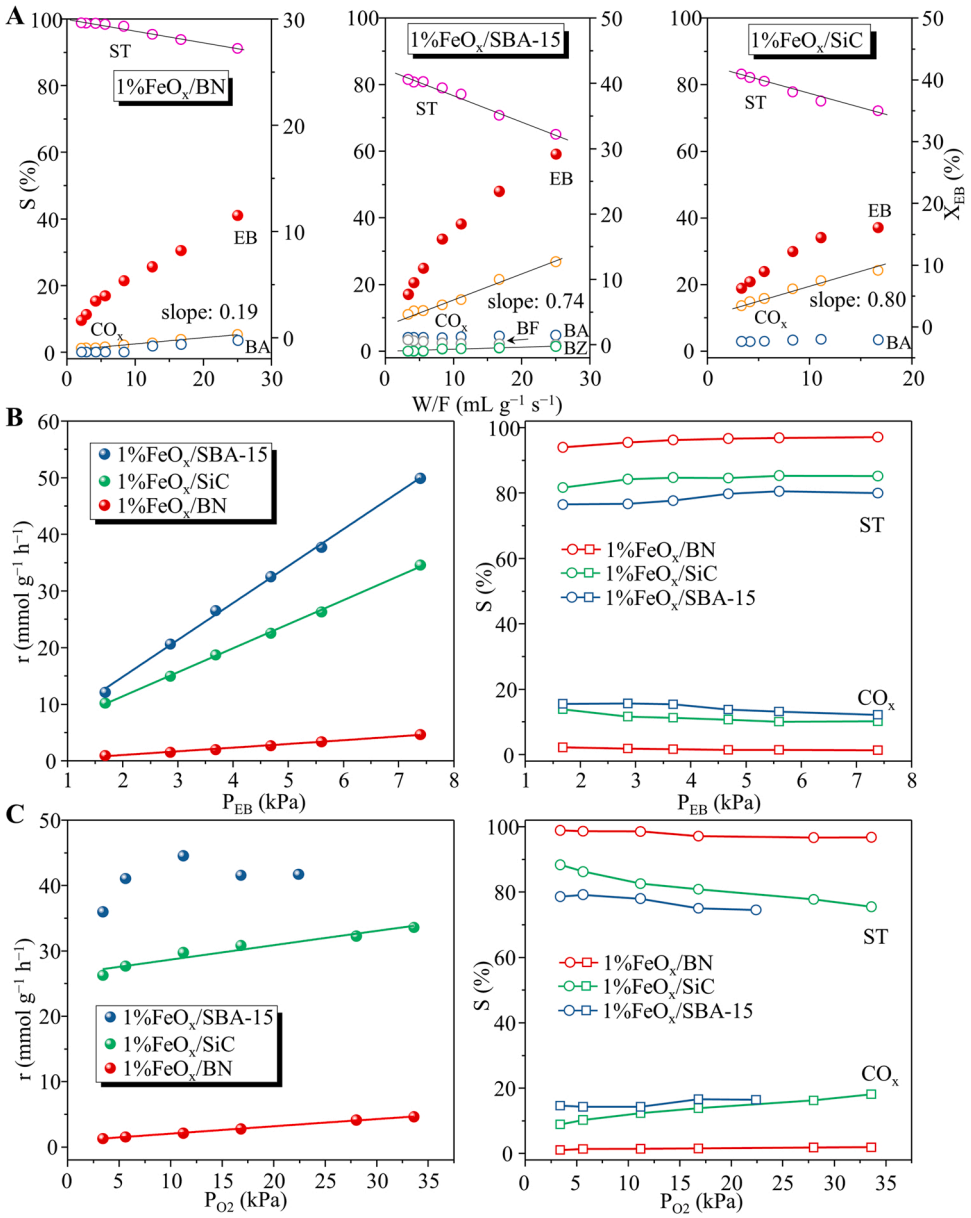

Fig. 2. Kinetic studies for supported FeO_x catalysts. (A) Effect of contact time on catalytic behaviors for the oxidative dehydrogenation of ethylbenzene. Reaction conditions: 500 ℃, EB = 5.6 kPa, O_2/EB = 2, N_2 as balance, GHSV = 9000–300,000 mL g^{-1} h^{-1}; Effect of partial pressure of EB (B) and O_2 (C) on reaction rate. Reaction conditions: 500 ℃, EB = 1.6–7.3 kPa, O_2 = 2.8–33.6 kPa, N_2 as balance, GHSV = 40,000 mL g^{-1} h^{-1}.

could also reflect the degree of overoxidation reactions (mainly including the direct oxidation of ethylbenzene to CO_x and the oxidation of styrene to CO_x). The slope value decreased in the sequence of 1% FeO_x/SiC (0.80) > 1%FeO_x/SBA-15 (0.74) > 1%FeO_x/BN (0.19), suggesting that the overoxidation reactions were markedly suppressed over 1%FeO_x/BN, leading to the high selectivity of styrene. As shown in Fig. S6, the oxidation of intermediate styrene over the supported FeO_x catalysts was also conducted to evaluate the degree of overoxidation. The reaction conditions, styrene concentration, and the ratio of oxygen to styrene, were set to be close to the steady state of real ethylbenzene oxidative dehydrogenation. Over the 1%FeO_x/BN catalyst, the conversion of styrene was maintained at only 1–2% level during the tested period; while over the FeO_x/SBA-15 and FeO_x/SiC catalyst, the conversion of styrene reached 30–40% (Fig. S6), suggesting that the overoxidation of styrene was strongly restrained by 1%FeO_x/BN catalyst, which was consistent with the results of the contact time experiment. Given there is a near 8-h induction period for FeO_x/BN and FeO_x/SBA-15, a relatively rapid testing procedure (total time consumption < 2.5 h) was taken to minimize the effect of coke deposition (containing active quinone/carbonyl sites) in the value of activation energy. Thus, the activation energy over the supported FeO_x catalysts (Fig. S7), in the sequence: FeO_x/BN (150 kJ mol^{-1}) < FeO_x/SBA-15 (77 kJ mol^{-1}) ~ FeO_x/SiC (66 kJ mol^{-1}), could reflect that the FeO_x species on the BN support were more moderate in activating ethylbenzene molecules than that on SBA-15 and SiC supports at the initial stage, consistent with the initial EB conversion over these catalysts in Table 1 (in the sequence: FeO_x/BN (20%) < FeO_x/SBA-15 (42%) ~ FeO_x/SiC (42%)). Based on these results, one could speculate that the overoxidation of ethylbenzene and styrene to CO_x was prominently suppressed over 1%FeO_x/BN, benefiting the high styrene selectivity.

Fig. 2B and C respectively showed the effects of partial pressure of EB and O_2 on the rates of EB conversion and the product selectivity over supported FeO_x catalysts. Over all the catalysts, the rate of EB conversion increased with the increase in partial pressure of EB. Besides, at a

fixed partial pressure of O_2, an increase in P_{EB} increased the selectivity to ST and decreased that to CO_x. While the rate of EB conversion increased slowly with the increase of partial pressure of O_2 at a fixed P_{EB}. Over the 1%FeO_x/SBA-15 and 1%FeO_x/SiC catalysts, the selectivity to ST decreased and that to CO_x increased with increasing P_{O2}. For the 1% FeO_x/BN catalyst, the selectivity of ST and CO_x did not change significantly with the increase in partial pressure of O_2. Generally, increasing the oxygen partial pressure will increase the surface concentration of reversibly adsorbed electrophilic oxygen species (such as O_2^-, O_2^{2-} or O^-) that are in equilibrium with the gas phase oxygen. These highly active oxygen species are considered to mainly involve in non-selective oxidation reactions. The high styrene selectivity across the tested range of oxygen partial pressure over the 1%FeO_x/BN catalyst suggested that the generation of electrophilic oxygen species was inhibited.

3.3. Structural properties of FeO_x/BN

Fig. 3A showed the XRD patterns of supported FeO_x catalysts. No XRD diffraction peaks relative to Fe compounds were detected in the supported FeO_x catalysts as Fe content less than 1 wt%, suggesting that the FeO_x species probably were highly dispersed on these supports. Small diffraction peaks at 2θ of 32.8° and 35.4°, attributable to the (104) and (110) reflections of Fe_2O_3 (ICDD: 01-080-2377) were observed in the enlarged figure as Fe content increased to 3 wt%, indicating the emergence of Fe_2O_3 crystallites. As the content raised to 9 wt%, detectable Fe_2O_3 nanoparticles (~10 nm, calculated by Scherrer equation) were observed from the enlarged figure due to the severe agglomeration of the high loading amount. On the other hand, no XRD diffraction peaks for boron oxide were detected, indicating that the BN

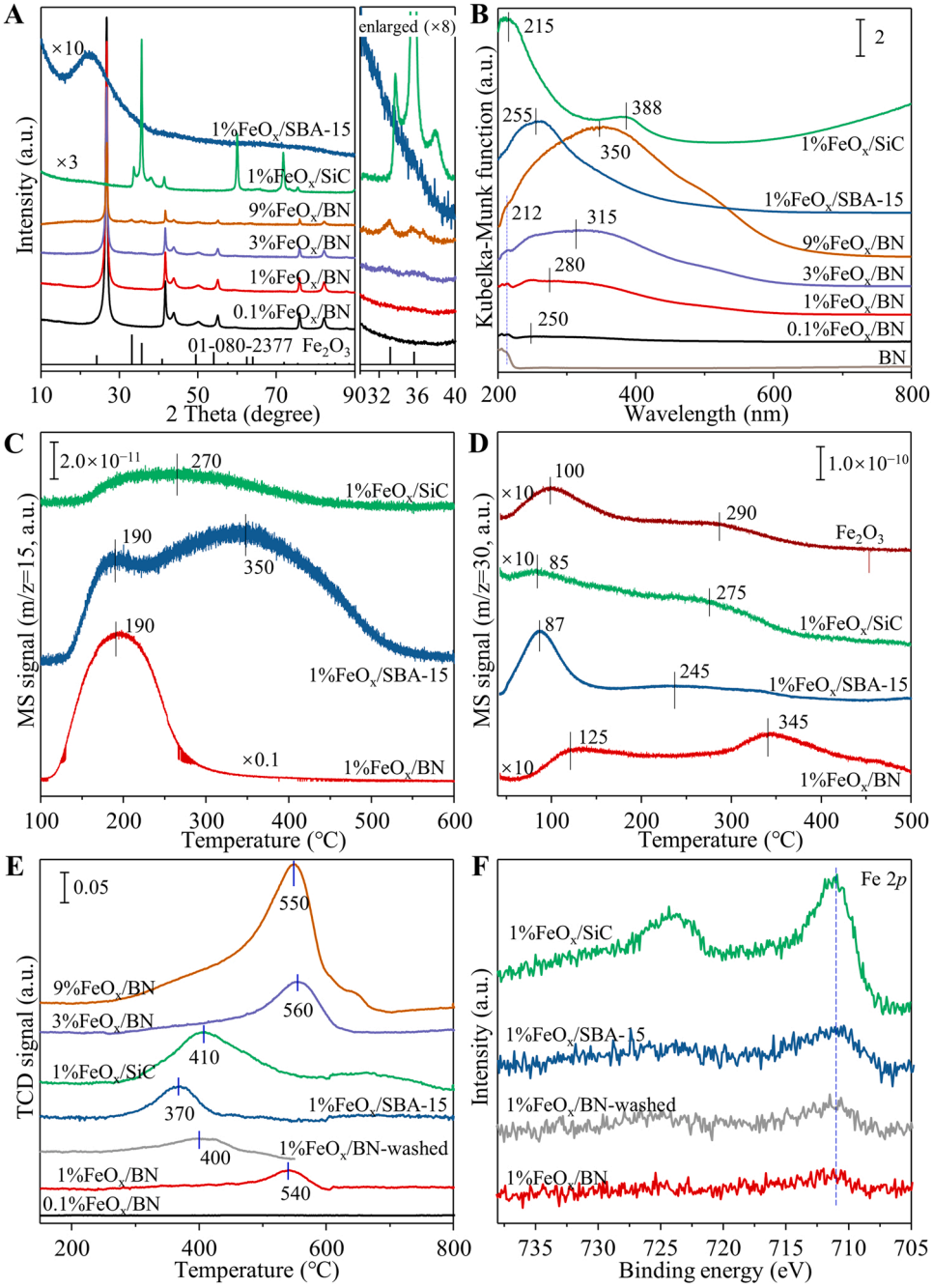

Fig. 3. Structural characterizations for supported FeO_x catalysts. (A) XRD patterns; (B) UV–vis DRS spectra; (C) NH_3-TPD profiles; (D) CH_3OH-TPD profiles; (E) H_2-TPR profiles; (F) XPS spectra of Fe 2*p*.

support was not oxidized to form crystalline boron oxide after air calcination.

As shown in Fig. 3B, the dispersion of iron oxide (FeO_x) species over BN, SBA-15, and SiC were further clarified by UV–vis DRS. The 1%FeO_x/SBA-15 exhibited a broad UV–vis absorption band at 255 nm, which could be attributed to the ligand (O^{2-}) to metal (Fe^{3+}) charge-transfer (LMCT) transition for small FeO_x clusters [21,47]. While the band at 388 nm over the 1%FeO_x/SiC sample could be assigned to oligomeric Fe species as Fe_xO_y [47]. For the 1%FeO_x/BN catalyst, the band at 212 nm could be assigned to the absorption of BN and the band at 282 nm could be attributed to the ligand (O^{2-}) to metal (Fe^{3+}) charge-transfer transition for FeO_x clusters. The deconvoluted UV–vis DRS further analyzed the FeO_x species of FeO_x/BN (Fig. S8). The absorption band at 255 nm in all the FeO_x/BN catalysts, which can be attributed to small FeO_x clusters. The bands at 320 nm and 385 nm can be ascribed to FeO_x clusters and oligomeric Fe species as Fe_xO_y, respectively [48]. The broad bands centered at 427 nm and 500 nm could be accordingly assigned to the large FeO_x species and crystalline Fe_2O_3 particles [48]. As shown in Table S2, the quantitative analysis of FeO_x species was also estimated based on the integral area of each species [47]. These results suggested that the 0.1%FeO_x/BN and 1%FeO_x/BN were dominated by FeO_x clusters, while a considerable amount of large FeO_x species and Fe_2O_3 particles presented in 3%FeO_x/BN and 9%FeO_x/BN, consistent with the results of XRD.

Fig. 3C and S9 show the NH_3-TPD profiles for supported FeO_x catalysts. For the bare BN support, only a desorption peak at 175 ℃ attributable to weak acid sites was observed (Fig. S9). After loading FeO_x, a broad desorption peak appeared at 190 ℃ with an increased amount of total acid sites from 40 to near 100 μmol NH_3 g^{-1} (Table 2), indicating the generation of new acid sites, which could result from Fe^{3+} (Lewis acid) on FeO_x species. As for 1%FeO_x/SBA-15, two overlapped desorption peaks at 190 and 350 ℃ were observed, which were respectively ascribed to the desorption of NH_3 from the Lewis and Brønsted acid sites [21]. It was speculated that the Lewis acid sites probably were in the result of FeO_x species, whereas the Brønsted acid sites might derive from the disturbed –OH due to the strong interaction of a part of iron with the Si–OH [21]. The 1%FeO_x/SiC sample showed a flat and broad desorption peak at 270 ℃ possibly due to the large FeO_x species.

Methanol was used as a probe molecule to determine the redox sites on the catalysts since the formaldehyde would be formed over these sites [49]. As shown in Fig. 3D, two formaldehyde formation peaks at 125 and 345 ℃ were observed over the 1%FeO_x/BN, which were much higher than that over 1%FeO_x/SBA-15 (87 and 245 ℃) and 1%FeO_x/SiC (87 and 275 ℃), suggesting that the redox reactivity of 1%FeO_x/BN was lower than that of 1%FeO_x/SBA-15 and 1%FeO_x/SiC.

As shown in Fig. 3E, the TPR technique was further used to probe the oxygen reactivity of supported FeO_x catalysts. Only one reduction peak at 540 ℃ was observed for the 1%FeO_x/BN catalyst, whereas the reduction peak for 1%FeO_x/SBA-15 and 1%FeO_x/SiC was at 370 and 410 ℃, respectively. The much higher reduction temperature of 1% FeO_x/BN catalyst suggested there existed a strong interaction between the iron species and the BN support [50,51], i.e., FeO_x clusters or Fe^{3+} ions, likely since the formation of the BO_x species that covered the FeO_x species. Given the water-solubility of BO_x species, the hot water washed sample, denote as 1%FeO_x/BN-washed, was also prepared. As shown in Fig. S10, the shoulder peaks at 192.2 eV in the B 1 s spectra were attributable to B−O bonding, indicating the presence of BO_x species. After water washing treatment, the fitted percentage of the B−O component decreased from 5.3% to 3.5% and the atomic ratio of Fe/B increased from 0.00275 to 0.00458, suggesting that a part of BO_x species was removed and more FeO_x species was exposed. Moreover, as shown in Fig. 3E, the reduction temperature of 1%FeO_x/BN-washed sample decreased to 400 ℃, which was close to the temperature of 1% FeO_x/SBA-15 (~370 ℃) and 1%FeO_x/SiC (~410 ℃) catalysts and was 140 ℃ lower than that of pristine 1%FeO_x/BN catalyst, indicating that the formed thin BO_x species was likely the origin of the strong interaction between the iron oxide species and BN support. Due to such interaction, the reactivity of lattice oxygen with respect to FeO_x species was markedly mitigated. Nucleophilic lattice oxygen species in reducible oxides are generally considered to be responsible for oxidative dehydrogenation of ethylbenzene. The low reactivity of lattice oxygen species could cause a relatively low activity, which was consistent with the relatively lower initial EB conversion and low O_2 conversion of 1% FeO_x/BN than that of 1%FeO_x/SBA-15 and 1%FeO_x/SiC (~20% < 42% = 42%, Table 1). The size influence of FeO_x species in their reducibility was further investigated by altering the loading amount of iron. No obvious reduction peak was observed for 0.1%FeO_x/BN catalyst possible due to the low loading of iron. The main reduction peak at ~550 ℃ was observed for other FeO_x/BN catalysts. As the iron content increased, the onset temperature respectively shifted to ~300 ℃ for 3%FeO_x/BN and ~250 ℃ for 9%FeO_x/BN, suggesting that the lattice oxygen species with higher reactivity existed in the larger FeO_x domains, which were consistent with the catalytic results of higher initial EB conversion and lower ST selectivity over these catalysts (Table 1). Besides, as listed in Table 2, the quantities of H_2 consumption for FeO_x/BN catalysts were much lower than the theoretical values (in parenthesis), implying the low oxygen reactivity of FeO_x/BN catalysts is possibly due to the strong interaction between FeO_x and BO_x species.

The oxidation states of the Fe species in the catalysts were determined by XPS, and the results are shown in Fig. 3F. Fe 2p peaks were at the same binding energy for all supported FeO_x catalysts and the oxidation state was at Fe^{3+}.

Fig. 4 and S11 show the TEM images of the FeO_x/BN catalysts. No obvious Fe_2O_3 nanoparticles were found over 1%FeO_x/BN possibly due to the low loading amount of iron. For the 9%FeO_x/BN sample, nanoparticles were observed with sizes of 15 nm and surrounded by BO_x species (circled in Fig. 4C). Fig. S12 displayed the nitrogen sorption isotherms of FeO_x/BN catalysts. The type-IV isotherms with an H2 hysteresis loop indicated the mesoporous characteristics of FeO_x/BN catalysts, which might be formed by the stack of small particles. The BET surface areas of the supported FeO_x catalysts were listed in Table 2.

Structural characterizations of spent catalysts were also conducted. As shown in Fig. S13, no significant changes in the diffraction of FeO_x species were observed after the time on stream reaction. Whereas the new peaks at 14.5° and 27.7°, attributable to the diffraction of B_2O_3 (ICDD: 00-006-0297) were observed for the spent FeO_x/BN catalysts, indicating that the amount of BO_x species would increase, even leading to the formation of detectable B_2O_3. The results of TEM (Fig. S14) suggested the aggregation of FeO_x species after a long-term reaction over 1%FeO_x/BN. The oxidation states of Fe species on spent catalysts were kept at + 3, but the intensity of signals was lower than that of fresh samples possibly due to the coke deposition on the surface (Fig. S15A). The C 1 s spectra (Fig. S15B, C, and Table S3) indicated the similar carbonaceous species over the spent 1%FeO_x/BN and 1%FeO_x/SBA-15 catalysts.

Table 2
Some properties of supported FeO_x catalysts.

Catalysts	S_{BET} (m^2 g^{-1})	H_2 consumption (μmol H_2 g^{-1})	Total acid sites (μmol NH_3 g^{-1})	Fe density (Fe nm^{-2})
0.1%FeO_x/BN	73.8	ND[a]	96	0.05
1%FeO_x/BN	71.2	53 (186)[b]	122	0.53
1%FeO_x/BN-washed	105	54	–	–
3%FeO_x/BN	64.2	149 (558)[b]	100	1.76
9%FeO_x/BN	57.5	464 (1674)[b]	115	5.89
1%FeO_x/SBA-15	730	71 (186)[b]	–	–
1%FeO_x/SiC	26	152 (186)[b]	–	–
BN	66.7	ND[a]	40	ND[a]

[a] ND stands for not detected.
[b] Values in parenthesis are quantity of theoretical H_2 consumption.

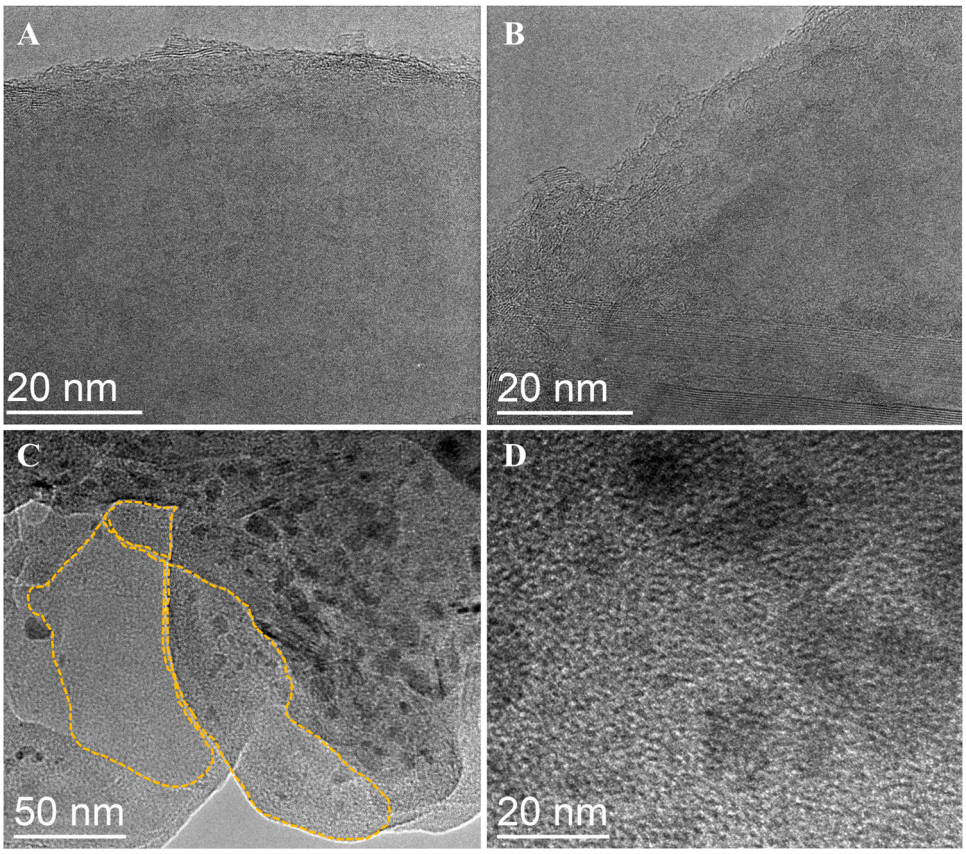

Fig. 4. TEM images of catalysts. (A) and (B) 1%FeO_x/BN; (C) and (D) 9%FeO_x/BN.

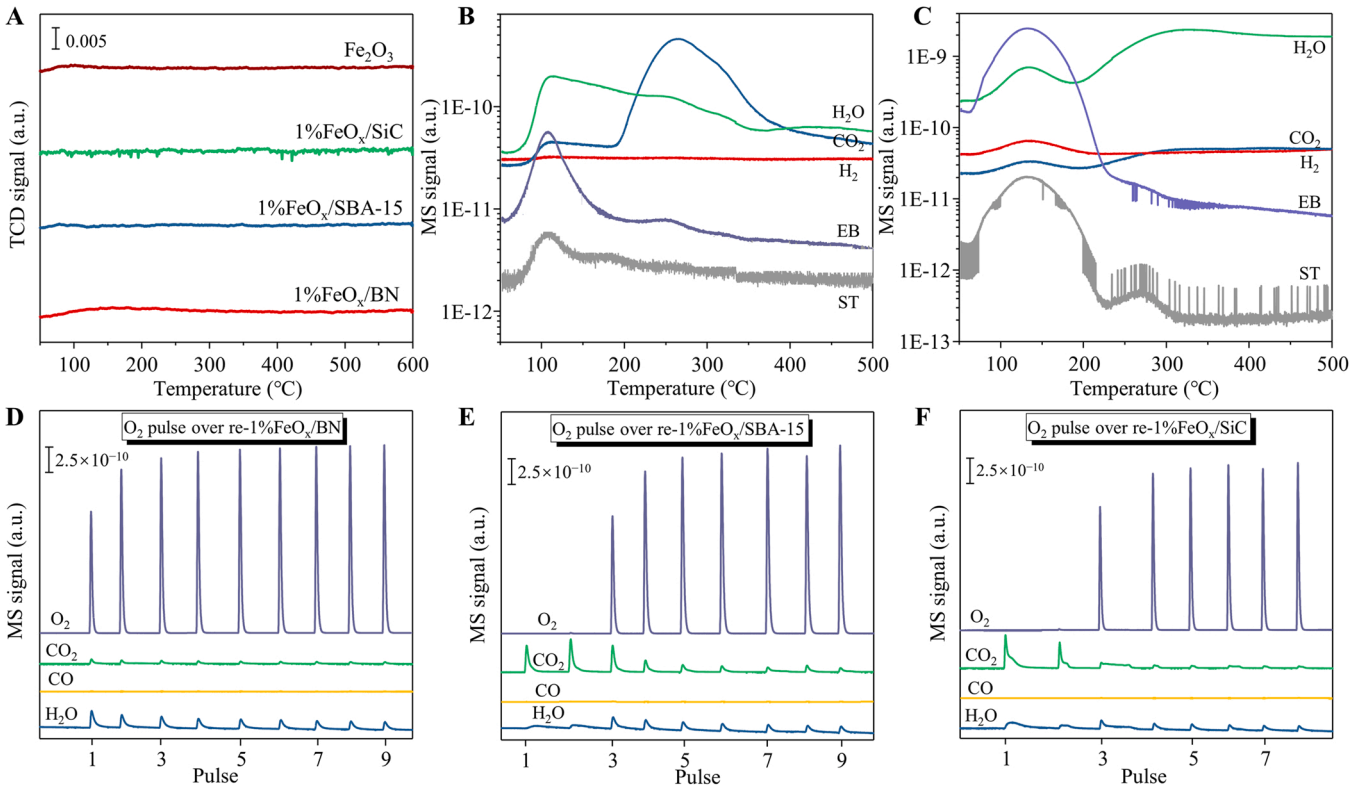

Fig. 5. (A) O_2-TPD profiles for FeO_x-based catalysts. EB-TPD profiles for 1%FeO_x/BN (B) and 1%FeO_x/SBA-15 (C). Reoxidation behavior of O_2 pulse over the EB-reduced supported FeO_x catalysts. (D) re-1%FeO_x/BN; (E) re-1%FeO_x/SBA-15; (F) re-1%FeO_x/SiC. Reaction conditions: 500 ℃, 100 mg, 5.6%EB/He, 10%O_2/He, V_{pulse} = 0.8 mL.

3.4. Reoxidation behavior of FeO_x/BN

The lattice oxygen has been proposed to account for the oxidative dehydrogenation of ethylbenzene over reducible metal oxide catalysts including FeO_x-based catalysts [52], which undergoes reduction (by EB) and reoxidation (by O_2) cycles. Among them, the reoxidation of catalysts, i.e., the replenishment of lattice oxygen in oxide from gas oxygen, has been regarded as a faster and more unmanageable step than the reduction step [10], usually causing the overoxidation reactions. Thus, studies on the process of reoxidation could be helpful to understand the reaction mechanism. O_2-TPD was first used to study the activation of oxygen over these FeO_x-based catalysts (Fig. 5A and S16). No signal of oxygen was detected, suggesting that these FeO_x species likely were in a stable valence state and could not directly activate the oxygen molecule. EB-TPD (Fig. 5B and C) was then verified the accessibility of FeO_x species. On the other hand, the supported FeO_x catalysts were reduced by EB/He pulses at 500 ℃ until the EB signal was unchanged, followed by purging with He at the same temperature for 1 h (the catalysts were denoted as re-FeO_x/support). Then, the in situ O_2 pulse was carried out. As shown in Fig. 5D, if O_2 was pulsed into the re-1%FeO_x/BN catalyst at 500 ℃, an obvious signal of O_2 was observed, and both CO_2 and H_2O were immediately formed possibly due to gasification of coke deposition. And the signals of CO_2 and H_2O gradually decreased and the O_2 signal was gradually stable during subsequent pulses. While over re-1% FeO_x/SBA-15 and re-1%FeO_x/SiC catalysts (Fig. 5E and F), the first two O_2 pulses were totally consumed, and then the O_2 signal gradually became stable. This indicated that the reoxidation process of re-1% FeO_x/BN was more moderate than that of re-1%FeO_x/SBA-15 and re-1% FeO_x/SiC catalysts, which could reduce the occurrence of overoxidation and result in a high styrene selectivity.

4. Discussion

4.1. Possible reaction pathways over supported FeO_x catalysts

The analyses of the changes of product distributions with the contact time provided useful information on speculating the reaction pathway. Over the 1%FeO_x/BN catalyst, styrene was deduced to be the major product since the near 100% selectivity of styrene as contact time approached zero (Fig. 2A), indicating that the direct oxidation of ethylbenzene to CO_x was inhibited. The increase in the contact time decreased the selectivity of styrene and increased that of benzaldehyde and CO_x. The low slope (0.19) of CO_x selectivity versus contact time reflected that the reaction channel of styrene to CO_x was also suppressed over the 1%FeO_x/BN catalyst. This suppression was further confirmed by the low conversion (< 2%) using styrene as a reactant (Fig. S6). Besides, the selectivity of styrene remained unchanged under the O_2-rich condition (Fig. 2C). These results allow one to speculate that the primary product over the 1%FeO_x/BN catalyst was styrene and the overoxidation reactions were strongly suppressed even under the O_2-rich condition. The small amount of benzaldehyde was the partial oxidation product (a secondary product) from styrene, and the other secondary product, CO_x may be generated from the consecutive oxidation of styrene or benzaldehyde (Scheme 1A). On the other hand, the obvious induction period in the time-on-stream test suggested that the coke deposition played a significant role in enhancing the activity (Fig. 1 and S1). In other words, the pathways consisted of parallel and consecutive reactions for the selective oxidation of ethylbenzene over the 1%FeO_x/BN catalyst. One is the oxidative dehydrogenation (ODH) route to form styrene, and the suppressed parallel or consecutive route to form CO_x from ethylbenzene or styrene. Styrene could be converted further to benzaldehyde and coke deposition. The coke deposition could also act as a catalyst for oxidative dehydrogenation of ethylbenzene.

For 1%FeO_x/SBA-15, both styrene and CO_x were formed as major products (selectivity: 80% for styrene; 10% for CO_x) at short contact times (Fig. 2A). Benzaldehyde, benzofuran, and benzene were also formed with relatively low selectivities in the initial stage. The increase in the contact time decreased the selectivity to styrene and increased that to CO_x. The higher conversion (30–40%) of styrene oxidation (Fig. S6) and lower selectivity of styrene under the O_2-rich conditions (Fig. 2C) further suggested that the severe overoxidation reactions occurred over the 1%FeO_x/SBA-15 catalyst. Similar behaviors were also observed over the 1%FeO_x/SiC catalyst. As summarized in Scheme 1B and S1, the direct oxidation of ethylbenzene to CO_x and the overoxidation of styrene to CO_x catalyzed by the active FeO_x species were the possible reasons for the low selectivity for styrene over the 1%FeO_x/SBA-15 and 1%FeO_x/SiC catalysts.

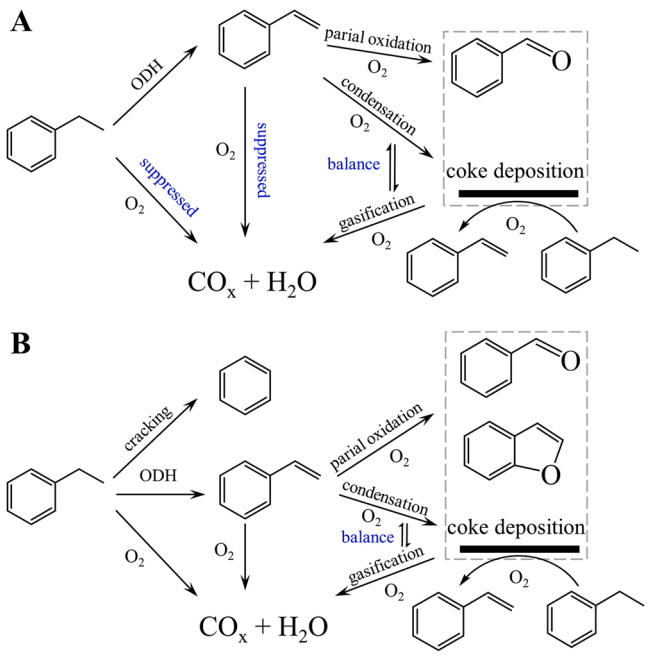

Scheme 1. Possible main reaction pathways for the oxidative dehydrogenation of ethylbenzene. (A) 1%FeO_x/BN; (B) 1%FeO_x/SBA-15.

4.2. Role of FeO_x, BN and coke

To compare and elucidate the role of FeO_x, BN and deposited coke, the 1%FeO_x/BN-24 h-H and 1%FeO_x/BN-washed samples were prepared and tested. For clarity, the catalytic performance over 1%FeO_x/BN was also shown in Fig. 6A. The 1%FeO_x/BN catalyst showed a stable catalytic performance after an induction period (Fig. 1), indicating the important function of the deposited coke in maintaining stable performance. However, the role of FeO_x species under the steady state was not clear. After removing the FeO_x species of the 1%FeO_x/BN-24 h sample by a diluted hydrochloric acid, a dramatic decrease from 40% to 15% in EB conversion in the first 2 h was observed (Fig. 6B). It is reported the dehydrogenation activity would be augmented by injecting a chlorine-containing compound into the reaction stream [53]. Thus, one could speculate the decrease in activity was in the result of the gasification of coke deposition, causing the dramatic decrease in the number of the active carbonyl/quinone sites. The optical photographs of fresh and spent 1%FeO_x/BN-24 h-H (Fig. S17) also showed the gasification of coke deposition during the ODH reaction. The removal of FeO_x could reduce the total acid sites and the weak-acid-strength sites derived from Fe^{3+}, which could dramatically decelerate the coke deposition from styrene, indicating the gasification of coke deposition was dominated under the O_2-riched conditions. Combining the catalytic results before and after removing FeO_x species, one could speculate the FeO_x species would maintain stable performance by balancing the coke deposition and its gasification during the reaction process.

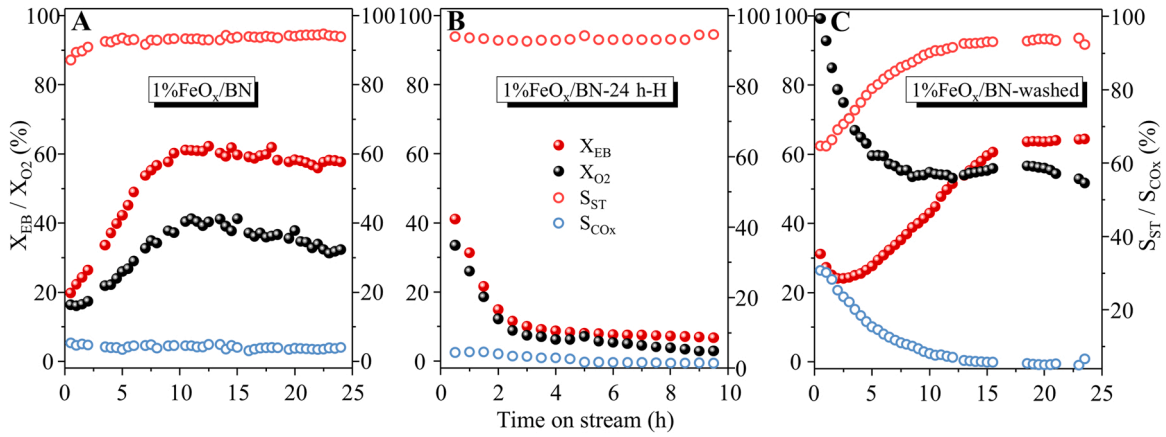

Fig. 6. Catalytic performance of oxidative dehydrogenation of ethylbenzene over supported FeO_x catalysts. (A) 1%FeO_x/BN; (B) 1%FeO_x/BN-24 h-H; (C) 1%FeO_x/BN-washed. Reaction conditions: 500 ℃, EB = 5.6 kPa, O_2/EB = 2, N_2 as balance, GHSV = 6000 mL g^{-1} h^{-1}.

The catalytic behaviors of the BO_x-removed 1%FeO_x/BN sample (1% FeO_x/BN-washed) also provided important information. As shown in Fig. 6C, the initial EB conversion and O_2 conversion respectively reached 30% and 100%, which were higher than that of pristine 1%FeO_x/BN (20% and 16%). While the initial selectivity of ST (~62%) and CO_x (~27%) were close to that of 1%FeO_x/SBA-15, 1%FeO_x/SiC, and bulk Fe_2O_3 samples (Table 1 and Fig. S1). Besides, the 1%FeO_x/BN-washed sample also showed as high as 30% conversion of styrene in the styrene oxidation reaction (Fig. S18). These results suggested that significant surface BO_x species were removed after the water-washing and a part of active FeO_x species were re-exposed, leading to higher initial conversion of EB and O_2 as well as lower selectivity to ST and higher selectivity to CO_x, which were in accordance with the result of H_2-TPR (Fig. 3E). An obvious decrease in the conversion of EB at the first 3 h then followed by a 12-h induction period and a stable of conversion EB was observed (Fig. 6C). Combining the tendency of O_2 conversion, we would suggest that the number of highly active FeO_x species decreased probably due to the re-formation of BO_x species from BN support under ODH reaction conditions. These species seemed to play the role in the spatial isolation of active oxygen species, which is a key factor in the selective oxidation reactions as proposed by Grasselli [54].

The B_2O_3 modified FeO_x/SBA-15 catalysts were also prepared to elucidate the role of BO_x or BN. As shown in Table S4, the 100% O_2 conversion in the whole tested period suggested that the artificially added BO_x species, neither before or after impregnating FeO_x over SBA-15 support, could not comparably tune the reactivity of FeO_x species like the BO_x species derived from BN support. These results strongly revealed that BN support was a prerequisite to guarantee the strong interaction. In further, advanced characterization techniques and theoretical simulation are needed to deeply understand such strong interaction.

From these results, one could conclude that: In the initial stage, the conversion of EB might trigger via a simple surface redox (Mars van Krevelen) mechanism involving the Fe^{3+}/Fe^{2+} couple, in which the catalyst underwent the reduction by EB and reoxidation by O_2 cycles (Fig. 5 and S2). However, the strong interaction between the FeO_x species and BN support, probably stemmed from the BO_x species, moderated the oxygen reactivity of FeO_x species with a matched reduction and reoxidation process (Fig. 3D and E) and led to a low initial EB conversion and O_2 conversion along with high styrene selectivity (Table 1 and Figs. S1 and S2). Meanwhile, weak-acid-strength centers caused by Fe^{3+} in FeO_x clusters could accelerate the precipitation of coke from styrene onto the surface [46,53] and result in the formation of active carbonyl/quinone groups, giving rise to the increase in EB conversion (Figs. 1, S1, S2 and 6A). With the aid of FeO_x and BO_x species, the steady state between coke deposition and its gasification was achieved (Fig. 6C), and the quasi-stationary activity and styrene selectivity over a long period of time were attained.

5. Conclusion

In summary, the FeO_x/BN catalyst exhibits a high styrene selectivity of 94% at the ethylbenzene conversion of 60% and excellent durability under switched conditions. The strong interaction between FeO_x species and BN support has been demonstrated in which FeO_x are covered by BO_x species derived from the BN support under air calcination or ODH reaction process. Such BO_x could moderate the oxygen reactivity of FeO_x species and achieve a matched reduction and reoxidation process in the ODH reaction, leading to a high styrene selectivity. The present study not only provides a promising catalyst for the production of commodity styrene in an energy-saving and eco-friendly way, but also broadens the SMSI concept from metal towards metal oxide in the oxidative atmosphere, especially over BN support.

CRediT authorship contribution statement

Jian Sheng: Investigation, Formal analysis, Writing – original draft. **Wen-Cui Li**: Formal analysis, Conceptualization, Writing – review & editing. **Wen-Duo Lu**: Formal analysis. **Bing Yan**: Formal analysis. **Bin Qiu**: Formal analysis. **Xin-Qian Gao**: Formal analysis. **Rui-Ping Zhang**: Investigation. **Shu-Zhen Zhou**: Investigation. **An-Hui Lu**: Conceptualization, Supervision, Funding acquisition, Writing – review & editing.

Declaration of Competing Interest

The authors declare that they have no known competing financial interests or personal relationships that could have appeared to influence the work reported in this paper.

Acknowledgments

This study was supported by the State Key Program of National Natural Science Foundation of China (21733002), National Key Research and Development Project (2018YFA0209404).

Appendix A. Supporting information

Supplementary data associated with this article can be found in the online version at doi:10.1016/j.apcatb.2022.121070.

References

[1] F. Cavani, F. Trifirò, Alternative processes for the production of styrene, Appl. Catal. A Gen. 133 (1995) 219–239.

[2] S. Jarczewski, M. Drozdek, P. Michorczyk, C. Cuadrado-Collados, J. Gandara-Loe, J. Silvestre-Albero, L. Lityńska-Dobrzyńska, P. Kuśtrowski, On the catalytic role of superficial VO_x species and coke deposited on mesoporous MgO replica in oxidative dehydrogenation of ethylbenzene, Appl. Surf. Sci. 504 (2020), 144336.

[3] J. Sheng, B. Yan, B. He, W.-D. Lu, W.-C. Li, A.-H. Lu, Nonmetallic boron nitride embedded graphitic carbon catalyst for oxidative dehydrogenation of ethylbenzene, Catal. Sci. Technol. 10 (2020) 1809–1815.

[4] W. Liu, B. Chen, X. Duan, K.-H. Wu, W. Qi, X. Guo, B. Zhang, D. Su, Molybdenum carbide modified nanocarbon catalysts for alkane dehydrogenation reactions, ACS Catal. 7 (2017) 5820–5827.

[5] H. Ba, J. Luo, Y. Liu, C. Duong-Viet, G. Tuci, G. Giambastiani, J.-M. Nhut, L. Nguyen-Dinh, O. Ersen, D.S. Su, C. Pham-Huu, Macroscopically shaped monolith of nanodiamonds @ nitrogen-enriched mesoporous carbon decorated SiC as a superior metal-free catalyst for the styrene production, Appl. Catal. B Environ. 200 (2017) 343–350.

[6] F.M. Bautista, J.M. Campelo, D. Luna, J.M. Marinas, R.A. Quirós, A.A. Romero, Screening of amorphous metal–phosphate catalysts for the oxidative dehydrogenation of ethylbenzene to styrene, Appl. Catal. B Environ. 70 (2007) 611–620.

[7] K.N. Rao, B.M. Reddy, B. Abhishek, Y.-H. Seo, N. Jiang, S.-E. Park, Effect of ceria on the structure and catalytic activity of V_2O_5/TiO_2–ZrO_2 for oxidehydrogenation of ethylbenzene to styrene utilizing CO_2 as soft oxidant, Appl. Catal. B Environ. 91 (2009) 649–656.

[8] J. Sheng, W.-C. Li, Y.-R. Wang, W.-D. Lu, B. Yan, B. Qiu, X.-Q. Gao, S.-Q. Cheng, L. He, A.-H. Lu, Coproduction of styrene and benzaldehyde over a boron nitride-supported monomeric MoO_x catalyst, J. Catal. 400 (2021) 265–273.

[9] S. Chen, L. Zeng, R. Mu, C. Xiong, Z.J. Zhao, C. Zhao, C. Pei, L. Peng, J. Luo, L. S. Fan, J. Gong, Modulating lattice oxygen in dual-functional Mo-V-O mixed oxides for chemical looping oxidative dehydrogenation, J. Am. Chem. Soc. 141 (2019) 18653–18657.

[10] C.A. Carrero, R. Schloegl, I.E. Wachs, R. Schomaecker, Critical literature review of the kinetics for the oxidative dehydrogenation of propane over well-defined supported vanadium oxide catalysts, ACS Catal. 4 (2014) 3357–3380.

[11] W. Qi, P. Yan, D.S. Su, Oxidative dehydrogenation on nanocarbon: Insights into the reaction mechanism and kinetics via in situ experimental methods, Acc. Chem. Res. 51 (2018) 640–648.

[12] W. Liu, C. Wang, F. Herold, B.J.M. Etzold, D. Su, W. Qi, Oxidative dehydrogenation on nanocarbon: effect of heteroatom doping, Appl. Catal. B Environ. 258 (2019), 117982.

[13] R. Han, J. Diao, S. Kumar, A. Lyalin, T. Taketsugu, G. Casillas, C. Richardson, F. Liu, C.W. Yoon, H. Liu, X. Sun, Z. Huang, Boron nitride for enhanced oxidative dehydrogenation of ethylbenzene, J. Energy Chem. 57 (2021) 477–484.

[14] L. Zeng, Z. Cheng, J.A. Fan, L.-S. Fan, J. Gong, Metal oxide redox chemistry for chemical looping processes, Nat. Rev. Chem. 2 (2018) 349–364.

[15] B. Sarkar, R. Goyal, L.N. Sivakumar Konathala, C. Pendem, T. Sasaki, R. Bal, MoO3 nanoclusters decorated on TiO_2 nanorods for oxidative dehydrogenation of ethane to ethylene, Appl. Catal. B Environ. 217 (2017) 637–649.

[16] Y.S. Yun, M. Lee, J. Sung, D. Yun, T.Y. Kim, H. Park, K.R. Lee, C.K. Song, Y. Kim, J. Lee, Y.-J. Seo, I.K. Song, J. Yi, Promoting effect of cerium on MoVTeNb mixed oxide catalyst for oxidative dehydrogenation of ethane to ethylene, Appl. Catal. B Environ. 237 (2018) 554–562.

[17] B. Beck, M. Harth, N.G. Hamilton, C. Carrero, J.J. Uhlrich, A. Trunschke, S. Shaikhutdinov, H. Schubert, H.-J. Freund, R. Schlögl, J. Sauer, R. Schomäcker, Partial oxidation of ethanol on vanadia catalysts on supporting oxides with different redox properties compared to propane, J. Catal. 296 (2012) 120–131.

[18] T.W. van Deelen, C. Hernández Mejía, K.P. de Jong, Control of metal-support interactions in heterogeneous catalysts to enhance activity and selectivity, Nat. Catal. 2 (2019) 955–970.

[19] J. Dong, Q. Fu, H. Li, J. Xiao, B. Yang, B. Zhang, Y. Bai, T. Song, R. Zhang, L. Gao, J. Cai, H. Zhang, Z. Liu, X. Bao, Reaction-induced strong metal-support interactions between metals and inert boron nitride nanosheets, J. Am. Chem. Soc. 142 (2020) 17167–17174.

[20] T. Song, J. Dong, R. Li, X. Xu, M. Hiroaki, B. Yang, R. Zhang, Y. Bai, H. Xin, L. Lin, R. Mu, Q. Fu, X. Bao, Oxidative strong metal-support interactions between metals and inert boron nitride, J. Phys. Chem. Lett. 12 (2021) 4187–4194.

[21] S. Yang, W. Zhu, Q. Zhang, Y. Wang, Iron-catalyzed propylene epoxidation by nitrous oxide: effect of boron on structure and catalytic behavior of alkali metal ion-modified FeOx/SBA-15, J. Catal. 254 (2008) 251–262.

[22] Z. He, H. Lin, P. He, Y. Yuan, Effect of boric oxide doping on the stability and activity of a Cu–SiO_2 catalyst for vapor-phase hydrogenation of dimethyl oxalate to ethylene glycol, J. Catal. 277 (2011) 54–63.

[23] J.T. Grant, C.A. Carrero, F. Goeltl, J. Venegas, P. Mueller, S.P. Burt, S.E. Specht, W. P. McDermott, A. Chieregato, I. Hermans, Selective oxidative dehydrogenation of propane to propene using boron nitride catalysts, Science 354 (2016) 1570–1573.

[24] L. Shi, D. Wang, W. Song, D. Shao, W.-P. Zhang, A.-H. Lu, Edge-hydroxylated boron nitride for oxidative dehydrogenation of propane to propylene, ChemCatChem 9 (2017) 1788–1793.

[25] L. Shi, B. Yan, D. Shao, F. Jiang, D. Wang, A.-H. Lu, Selective oxidative dehydrogenation of ethane to ethylene over a hydroxylated boron nitride catalyst, Chin. J. Catal. 38 (2017) 389–395.

[26] J.T. Grant, W.P. McDermott, J.M. Venegas, S.P. Burt, J. Micka, S.P. Phivilay, C. A. Carrero, I. Hermans, Boron and boron-containing catalysts for the oxidative dehydrogenation of propane, ChemCatChem 9 (2017) 3623–3626.

[27] R. Huang, B. Zhang, J. Wang, K.-H. Wu, W. Shi, Y. Zhang, Y. Liu, A. Zheng, R. Schlögl, D.S. Su, Direct insight into ethane oxidative dehydrogenation over boron nitrides, ChemCatChem 9 (2017) 3293–3297.

[28] B. Yan, W.-C. Li, A.-H. Lu, Metal-free silicon boride catalyst for oxidative dehydrogenation of light alkanes to olefins with high selectivity and stability, J. Catal. 369 (2019) 296–301.

[29] Z. Liu, B. Yan, S. Meng, R. Liu, W.D. Lu, J. Sheng, Y. Yi, A.H. Lu, Plasma tuning local environment of hexagonal boron nitride for oxidative dehydrogenation of propane, Angew. Chem. Int. Ed. 60 (2021) 19691–19695.

[30] W.-D. Lu, D. Wang, Z. Zhao, W. Song, W.-C. Li, A.-H. Lu, Supported boron oxide catalysts for selective and low-temperature oxidative dehydrogenation of propane, ACS Catal. 9 (2019) 8263–8270.

[31] Q. Liu, Y. Wu, F. Xing, Q. Liu, X. Guo, C. Huang, B_2O_3@BPO_4 sandwich-like hollow spheres as metal-free supported liquid-phase catalysts, J. Catal. 381 (2020) 599–607.

[32] B. Qiu, F. Jiang, W.-D. Lu, B. Yan, W.-C. Li, Z.-C. Zhao, A.-H. Lu, Oxidative dehydrogenation of propane using layered borosilicate zeolite as the active and selective catalyst, J. Catal. 385 (2020) 176–182.

[33] J. Sheng, B. Yan, W.-D. Lu, B. Qiu, X.-Q. Gao, D. Wang, A.-H. Lu, Oxidative dehydrogenation of light alkanes to olefins on metal-free catalysts, Chem. Soc. Rev. 50 (2021) 1438–1468.

[34] J. Tian, J. Tan, Z. Zhang, P. Han, M. Yin, S. Wan, J. Lin, S. Wang, Y. Wang, Direct conversion of methane to formaldehyde and CO on B_2O_3 catalysts, Nat. Commun. 11 (2020) 5693.

[35] D. Zhao, J. Feng, Q. Huo, N. Melosh, G.H. Fredrickson, B.F. Chmelka, G.D. Stucky, Triblock copolymer syntheses of mesoporous silica with periodic 50 to 300 angstrom pores, Science 279 (1998) 548–552.

[36] Y.-R. Liu, X. Li, W.-M. Liao, A.-P. Jia, Y.-J. Wang, M.-F. Luo, J.-Q. Lu, Highly active Pt/BN catalysts for propane combustion: the roles of support and reactant-induced evolution of active sites, ACS Catal. 9 (2019) 1472–1481.

[37] R.M. Freire, F.F. de Sousa, A.L. Pinheiro, E. Longhinotti, J.M. Filho, A.C. Oliveira, Pd.T.C. Freire, A.P. Ayala, A.C. Oliveira, Studies of catalytic activity and coke deactivation of spinel oxides during ethylbenzene dehydrogenation, Appl. Catal. A Gen. 359 (2009) 165–179.

[38] I. Melián-Cabrera, V. Zarubina, C. Nederlof, F. Kapteijn, M. Makkee, An in situ reactivation study reveals the supreme stability of γ-alumina for the oxidative dehydrogenation of ethylbenzene to styrene, Catal. Sci. Technol. 8 (2018) 3733–3736.

[39] L. Shi, D. Wang, A.-H. Lu, A viewpoint on catalytic origin of boron nitride in oxidative dehydrogenation of light alkanes, Chin. J. Catal. 39 (2018) 908–913.

[40] Y. Zhou, J. Lin, L. Li, X. Pan, X. Sun, X. Wang, Enhanced performance of boron nitride catalysts with induction period for the oxidative dehydrogenation of ethane to ethylene, J. Catal. 365 (2018) 14–23.

[41] A.M. Love, B. Thomas, S.E. Specht, M.P. Hanrahan, J.M. Venegas, S.P. Burt, J. T. Grant, M.C. Cendejas, W.P. McDermott, A.J. Rossini, I. Hermans, Probing the transformation of boron nitride catalysts under oxidative dehydrogenation conditions, J. Am. Chem. Soc. 141 (2019) 182–190.

[42] F. Cavani, N. Ballarini, A. Cericola, Oxidative dehydrogenation of ethane and propane: how far from commercial implementation? Catal. Today 127 (2007) 113–131.

[43] J.S. Tian, J.H. Lin, M.L. Xu, S.L. Wan, J.D. Lin, Y. Wang, Hexagonal boron nitride catalyst in a fixed-bed reactor for exothermic propane oxidation dehydrogenation, Chem. Eng. Sci. 186 (2018) 142–151.

[44] J. Wang, J. Diao, J. Zhang, Y. Zhang, H. Liu, D.S. Su, Few-layer sp^2 carbon supported on Al_2O_3 as hybrid structure for ethylbenzene oxidative dehydrogenation, Catal. Today 301 (2018) 32–37.

[45] H. Ba, Y. Liu, L. Truong-Phuoc, C. Duong-Viet, J.-M. Nhut, D.L. Nguyen, O. Ersen, G. Tuci, G. Giambastiani, C. Pham-Huu, N-doped food-grade-derived 3D mesoporous foams as metal-free systems for catalysis, ACS Catal. 6 (2016) 1408–1419.

[46] G. Emig, H. Hofmann, Action of zirconium-phosphate as a catalyst for the oxydehydrogenation of ethylbenzene to styrene, J. Catal. 84 (1983) 15–26.

[47] P. Chen, M. Jabłońska, P. Weide, T. Caumanns, T. Weirich, M. Muhler, R. Moos, R. Palkovits, U. Simon, Formation and effect of NH_4^+ intermediates in NH_3–SCR over Fe-ZSM-5 zeolite catalysts, ACS Catal. 6 (2016) 7696–7700.

[48] J. García-Aguilar, I. Miguel-García, J. Juan-Juan, I. Such-Basáñez, E. San Fabián, D. Cazorla-Amorós, Á. Berenguer-Murcia, One step-synthesis of highly dispersed iron species into silica for propylene epoxidation with dioxygen, J. Catal. 338 (2016) 154–167.

[49] M. Badlani, I.E. Wachs, Methanol: a "smart" chemical probe molecule, Catal. Lett. 75 (2001) 137–149.

[50] Y. Cao, P. Maitarad, M. Gao, T. Taketsugu, H. Li, T. Yan, L. Shi, D. Zhang, Defect-induced efficient dry reforming of methane over two-dimensional Ni/h-boron nitride nanosheet catalysts, Appl. Catal. B Environ. 238 (2018) 51–60.

[51] J. Wu, L. Wang, X. Yang, B. Lv, J. Chen, Support effect of the Fe/BN catalyst on Fischer–Tropsch performances: role of the surface B–O defect, Ind. Eng. Chem. Res. 57 (2018) 2805–2810.

[52] K. Saito, K. Okuda, N.O. Ikenaga, T. Miyake, T. Suzuki, Role of lattice oxygen of metal oxides in the dehydrogenation of ethylbenzene under a carbon dioxide atmosphere, J. Phys. Chem. A 114 (2010) 3845–3854.

[53] R. Fiedorow, W. Przystajko, M. Sopa, The nature and catalytic influence of coke formed on alumina - oxidative dehydrogenation of ethylbenzene, J. Catal. 68 (1981) 33–41.

[54] R.K. Grasselli, Fundamental principles of selective heterogeneous oxidation catalysis, Top. Catal. 21 (2002) 79–88.